International Journal of Heat and Fluid Flow 32 (2011) 402–412

Contents lists available at ScienceDirect

International Journal of Heat and Fluid Flow

journal homepage: www.elsevier.com/locate/ijhff

Effect of magnetic field on the buoyancy and thermocapillary driven convection of an electrically conducting fluid in an annular enclosure

M. Sankar [a,b,*], M. Venkatachalappa [c], Younghae Do [a]

[a] Department of Mathematics, Kyungpook National University, 1370 Sangyeok-Dong, Buk-Gu, Daegu 702-701, Republic of Korea
[b] Department of Mathematics, East Point College of Engineering and Technology, Bangalore 560 049, India
[c] UGC Centre for Advanced Studies in Fluid Mechanics, Department of Mathematics, Bangalore University, Bangalore 560 001, India

ARTICLE INFO

Article history:
Received 25 December 2009
Received in revised form 30 November 2010
Accepted 13 December 2010
Available online 8 January 2011

Keywords:
Magnetic field
Cylindrical annulus
Finite difference
Thermocapillary convection
Surface tension
Radii ratio

ABSTRACT

The main objective of this article is to study the effect of magnetic field on the combined buoyancy and surface tension driven convection in a cylindrical annular enclosure. In this study, the top surface of the annulus is assumed to be free, and the bottom wall is insulated, whereas the inner and the outer cylindrical walls are kept at hot and cold temperatures respectively. The governing equations of the flow system are numerically solved using an implicit finite difference technique. The numerical results for various governing parameters of the problem are discussed in terms of the streamlines, isotherms, Nusselt number and velocity profiles in the annuli. Our results reveal that, in tall cavities, the axial magnetic field suppresses the surface tension flow more effectively than the radial magnetic field, whereas, the radial magnetic field is found to be better for suppressing the buoyancy driven flow compared to axial magnetic field. However, the axial magnetic field is found to be effective in suppressing both the flows in shallow cavities. From the results, we also found that the surface tension effect is predominant in shallow cavities compared to the square and tall annulus. Further, the heat transfer rate increases with radii ratio, but decreases with the Hartmann number.

1. Introduction

Thermocapillary convection is a fluid motion driven by the surface tension variation at a free surface resulting from the thermal gradients along the surface. The combination of buoyancy and free surface shear frequently exhibits a complex flow field. These two forces may assist or compete with each other to dominate the flow field. In Czochralski crystal growth process, the convection may be driven either by a buoyancy due to density gradient caused by lateral heating, or a surface tension force due to temperature gradient along the free surface. The ever-growing demand for a high quality crystal material has resulted in a substantial research focused on the understanding, and eventually controlling the convection in material processing systems. Since the convective flow is the major cause of some macroscopic defects in the crystal produced, it is desirable to remove this deleterious flow. One of the effective methods to control a thermally induced flow is the magnetic damping, in which the applied magnetic field will generate a Lorentz force to damp the convective flow. The damping effect depends on the strength of the applied magnetic field and its orientation with respect to the convective flow direction. Substantial theoretical and numerical work thus far has appeared on the magnetic damping of natural convection.

Langlois (1985) has made a detailed review on the effect of an external magnetic field on Czochralski crystal growth. He concluded that when the magnetic Reynolds number is very small, it is not necessary to consider the complete MHD theory to investigate the Czochralski flow. A theoretical analysis of the effect of magnetic field on the source distribution in Czochralski grown crystals has been given by Kobayashi (1986). A review on the surface tension driven convection in the crystal growth melt flow has been carried out by Schwabe (1988). Ozoe and Okada (1989) have numerically investigated the effect of magnetic damping in a cubic enclosure. They found that the strongest damping effect is achieved when the magnetic field is applied perpendicular to the hot wall. Venkatachalappa and Subbaraya (1993) investigated natural convection in a rectangular enclosure in the presence of a vertical magnetic field. Their numerical results revealed that the temperature and velocity fields are significantly modified by the applied magnetic field. BenHadid and Henry (1997) studied the damping effect of a steady convection in a $4 \times 1 \times 1$ cavity with a magnetic field applied in different directions. Their results were in good agreement with the analytical predictions of Garandet et al. (1992) and Alboussière et al. (1996).

* Corresponding author. Tel.: +82 53 950 7951; fax: +82 53 950 7954.
E-mail address: manisankarir@yahoo.com (M. Sankar).

0142-727X/$ - see front matter © 2010 Elsevier Inc. All rights reserved.
doi:10.1016/j.ijheatfluidflow.2010.12.001

Nomenclature

A	aspect ratio
B_0	magnetic field strength
(B_{0r}, B_{0x})	magnetic field strength in (r, x) direction
D	annulus gap
(F_r, F_x)	electromagnetic force components in (r, x) direction
g	acceleration due to gravity
Har	Hartmann number due to radial magnetic field
Hax	Hartmann number due to axial magnetic field
L	height of the annulus
Ma	Marangoni number
Nu	Nusselt number
P	pressure
Pr	Prandtl number
Ra	Rayleigh number
T	dimensionless temperature
t	dimensional time
(r, x)	dimensional radial and axial co-ordinates
(R, X)	dimensionless radial and axial co-ordinates
(r_i, r_0)	radii of inner and outer cylinders
(u, v)	dimensional velocity components in (r, x) direction
(U, V)	dimensionless velocity components in (R, X) direction

Greek letters

β	coefficient of thermal expansion
γ	coefficient of surface tension
η^*	dimensional vorticity
η	dimensionless vorticity
θ	dimensional temperature
κ	thermal diffusivity
λ	radii ratio
ν	kinematic viscosity
ρ	fluid density
σ	surface tension
σ_e	electrical conductivity
τ	dimensionless time
ψ	dimensional stream function
Ψ	dimensionless stream function
$\Psi_{\max,s}$	maximum value of thermocapillary driven stream function

Subscripts

h	condition at hot wall
c	condition at cold wall.
0	reference state
max	maximum value

Carpenter and Homsy (1989) have studied the problem of combined buoyancy and thermocapillary convection in a differentially heated square cavity with a free surface. Numerical simulations of combined buoyancy and surface tension driven convection in a rectangular cavity have been performed by Rudraiah et al. (1995) in the presence of a magnetic field. They found that the average Nusselt number increases with Marangoni number, but decreases with Hartmann number. Some notable studies on the numerical simulation of combined buoyancy and/or thermocapillary convection in a differentially heated rectangular enclosures are due to Strani et al. (1983), Srinivasan and Basu (1986), Bergman and Ramadhyani (1986), Bergman and Keller (1988), Juel et al. (1999), Moessner and Mueller (1999) and Gelfgat and Bar-Yoseph (2001). The effect of magnetic field on the combined buoyancy and thermocapillary driven convection in a rectangular enclosure containing a heat generating substance has been numerically investigated by Hossain et al. (2005). Their study was mainly focused upon the magnetic field direction and the effect of a heat generation parameter on the flow and heat transfer. Ha and Kim (2005) investigated the transient molten pool geometry during a laser melting process with a deformable flat surface. The recent studies on the natural convection in rectangular enclosure under the influence of magnetic field are by Lee and Hyun (2005) and Sarris et al. (2005).

Vrentas et al. (1981) have studied the surface tension and buoyancy driven convection in a vertical circular cylinder for a wide range of aspect ratios. They determined the critical Marangoni and Rayleigh numbers, structure of convective motion, and nature of bifurcation branching. An experimental study of oscillatory thermocapillary convection in cylindrical containers with a heating wire placed along the axis of a vertical cylinder was performed by Kamotani et al. (1992). From the experimental results they have observed an oscillatory thermocapillary flow, beyond a certain temperature difference between the container wall and the heating wire. Schwabe et al. (2003) have performed microgravity experiments on the thermocapillary convection in a cylindrical annulus with a free liquid surface. They measured the critical temperature difference for the onset of temperature oscillations detecting hydrothermal waves. Sim et al. (2003) carried out numerical simulations of oscillatory thermocapillary convection in a cylindrical annulus with a free liquid surface and found a steady and axisymmetric convection at sufficiently low Reynolds numbers. Bauer and Eidel (2007) analytically investigated the effect of aspect and diameter ratios on the thermocapillary convection in an annular cylindrical container. Recently, Kim and Kim (2008) performed a numerical investigation of two-dimensional axisymmetric thermocapillary convection during laser melting processes with deformable free surfaces. More recently, Kakarantzas et al. (2009) demonstrated the effect of sinusoidal temperature on the magnetohydrodynamic natural convection in a cylindrical cavity.

Most of the previous studies found in the literature on the combined buoyancy and surface tension driven convection were concentrated either on a rectangular cavity, with or without a magnetic field, or on a cylindrical geometry without a magnetic field. However, to the best of our knowledge, the problem of combined buoyancy and surface tension driven convection in a vertical cylindrical annulus with a free surface has not yet been studied in the presence of a magnetic field. This problem attracts by its sheer existence and intellectual curiosity, but its treatment and investigation would be quite complex and expensive for the experiments. Thus the objective of the present numerical study is to investigate the effect of direction of magnetic field on the combined buoyancy and surface tension driven convection in a vertical cylindrical annulus, which is filled with an electrically conducting fluid.

2. Mathematical formulation

The physical configuration of the present study consists of a cylindrical annular enclosure formed by two vertical, concentric cylinders of inner and outer radii r_i and r_0, as shown schematically in Fig. 1. The inner and outer walls of the annulus are isothermal, but maintained at different temperatures, θ_h at the inner hot wall and θ_c at the outer cold wall, resulting in a radial temperature gradient. The free surface and bottom wall of the annulus are assumed to be adiabatic, and all the walls are electrically insulated. The

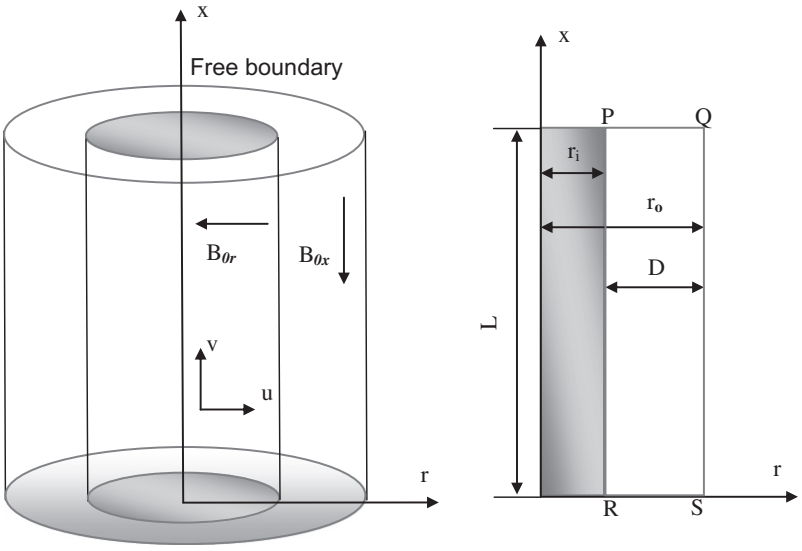

Fig. 1. Flow configuration and co-ordinate system.

annular cavity is filled with an electrically conducting low Prandtl number fluid, and is placed in a constant magnetic field. The fluid is assumed to be Newtonian with constant physical properties (kinematic viscosity υ, thermal diffusivity κ, density ρ), except for the density in the buoyancy term, which in the Boussinesq approximation linearly depends on the temperature in the axial momentum equation. Assuming the axi-symmetry, a semi-vertical plane, marked as PQRS in Fig. 1, is considered for the analysis.

The fluid is permeated by a uniform magnetic field B_0 either in the *r*- or *x*-direction. The effect of constant magnetic field is added through the Lorentz force to the momentum equation. For calculation of this magnetic damping term, the low magnetic Reynolds number approximation is used (Moreau, 1998). In this approximation, the induced magnetic field is considered to be very weak when compared with the external magnetic field B_0. This is true for low magnetic Reynolds number flows as those of liquid-metal flows used in laboratory scale experiments. A useful discussion for the validity limits of this approximation in natural convection flows can be found in Sarris et al. (2006). We also assumed that the surface tension coefficient on the upper boundary is assumed to vary linearly with the temperature, that is, $\sigma = \sigma_0 [1 - \gamma(\theta - \theta_0)]$, where $\gamma = (-1/\sigma_0)\frac{\partial \sigma}{\partial \theta}$ is the temperature coefficient of surface tension and the subscript 0 refers to the reference state. Further it is assumed that, the upper (free) boundary is flat and the fluid above the free surface is assumed to be a gas of negligible viscosity and conductivity, and hence it will not influence the flow and temperature fields in the fluid. Employing the above assumptions, the vorticity stream function form of the governing equations can be expressed as (Sankar et al., 2006):

$$\frac{\partial T}{\partial \tau} + \frac{U}{A}\frac{\partial T}{\partial R} + \frac{V}{A}\frac{\partial T}{\partial X} = \nabla^2 T, \tag{1}$$

$$\frac{\partial \eta}{\partial \tau} + \frac{U}{A}\frac{\partial \eta}{\partial R} + \frac{V}{A}\frac{\partial \eta}{\partial X} - \frac{U}{A}\left(\frac{D}{RD + r_i}\right)\eta = \mathrm{Pr}\nabla^2\eta - \mathrm{Pr}\left(\frac{D}{RD + r_i}\right)^2 \eta + \mathrm{Har}^2\frac{\partial V}{\partial R} - \frac{\mathrm{Hax}^2}{A^2}\frac{\partial U}{\partial X} + \mathrm{Ra}\frac{\partial T}{\partial R}, \tag{2}$$

$$\eta = \frac{1}{\mathrm{Pr}}\left(\frac{r_i}{DR + r_i}\right)\left[\frac{\partial^2 \Psi}{\partial R^2} - \left(\frac{D}{DR + r_i}\right)\frac{\partial \Psi}{\partial R} + \frac{1}{A^2}\frac{\partial^2 \Psi}{\partial X^2}\right], \tag{3}$$

$$U = \left(\frac{r_i}{DR + r_i}\right)\frac{\partial \Psi}{\partial X}, \quad V = -\left(\frac{r_i}{DR + r_i}\right)\frac{\partial \Psi}{\partial R}, \tag{4}$$

where $\eta = \frac{1}{\mathrm{Pr}}\left[\frac{1}{A^2}\frac{\partial U}{\partial X} - \frac{\partial V}{\partial R}\right]$ and $\nabla^2 = \frac{\partial^2}{\partial R^2} + \left(\frac{D}{DR + r_i}\right)\frac{\partial}{\partial R} + \frac{1}{A^2}\frac{\partial^2}{\partial X^2}$.

The unsteady terms are retained for the purpose of numerical calculations, and the large-time converged solutions will be taken as the steady state values. It may be noted Eqs. (1)–(4) of the current formulation can be readily converted to a rectangular cavity case by just substituting $D = 0$.

The non-dimensional variables used in the present study are given by

$$U = \frac{uD}{\kappa}A, \quad V = \frac{vL}{\kappa A}, \quad T = \frac{\theta - \theta_c}{\theta_h - \theta_c}, \quad R = \frac{r - r_i}{D},$$
$$X = \frac{x}{L}, \quad \tau = \frac{t\kappa}{D^2}, \quad \eta = \frac{\eta^* D^2}{\upsilon}, \quad \Psi = \frac{\psi}{r_i \kappa}, \quad D = r_o - r_i \tag{5}$$

The initial and boundary conditions in dimensionless form are:

$$\tau = 0: \quad U = V = T = 0, \quad \Psi = \eta = 0; \qquad 0 \leqslant R \leqslant 1, \quad 0 \leqslant X \leqslant 1.$$
$$\tau > 0: \quad \Psi = \frac{\partial \Psi}{\partial R} = 0, \quad T = 1; \quad R = 0,$$
$$\Psi = \frac{\partial \Psi}{\partial R} = 0, \quad T = 0; \quad R = 1,$$
$$\Psi = \frac{\partial \Psi}{\partial X} = 0, \frac{\partial T}{\partial X} = 0; \quad X = 0,$$
$$\Psi = \frac{\partial U}{\partial X} = \frac{\partial^2 \Psi}{\partial X^2} = 0, \frac{\partial T}{\partial X} = 0; \quad X = 1.$$

The dynamical condition on the upper free surface represents the balance between the shear stress and surface tension gradient, which is responsible for the establishment of thermocapillary flow in the cavity. We also assumed that the free surface of the annulus is maintained at adiabatic condition. This was a common assumption in the analysis of combined buoyancy and surface tension driven convection in finite enclosures with a free surface. In the convection heat transfer problems, the dominant heat transfer is due to free convection from the hot wall. The existing studies have estimated the heat loss by convection from the free surface to the surrounding gas, and found that the magnitude of heat loss from the free surface to the surrounding fluid is much lower than the heat transfer from the hot wall to the adjacent fluid. Therefore, the heat loss from the top free surface can be neglected and hence the adiabatic condition at the free surface was reasonable. This assumption has been used in many previous investigations in the literature (Bergman and Keller, 1988; Rudraiah et al., 1995; Hossain et al., 2005).

To solve the vorticity at next time levels, the boundary conditions on η has to be derived using the interior Ψ values (Roache, 1972). The value of vorticity on a solid boundary is deduced from the Taylor series expansion of the stream function Ψ near the walls. However, at the free surface, the vorticity boundary condition is derived from the dynamical condition between shear stress and surface tension gradient. The boundary conditions for the vorticity is:

$$\eta = \left(\frac{r_i}{\Pr(RD + r_i)}\right)\frac{\partial^2 \Psi}{\partial R^2}; \quad R = 0, \ R = 1 \text{ and } 0 \leqslant X \leqslant 1$$

$$\eta = \left(\frac{r_i}{A^2 \Pr(RD + r_i)}\right)\frac{\partial^2 \Psi}{\partial X^2}; \quad X = 0 \text{ and } 0 \leqslant R \leqslant 1$$

$$\eta = \frac{\partial U}{\partial X} = A\mathrm{Ma}\frac{\partial T}{\partial R}; \quad X = 1 \text{ and } 0 \leqslant R \leqslant 1.$$

In the above equations A, Ra, Pr, Har, Hax, Ma and λ are, respectively, the aspect ratio, the Rayleigh number, the Prandtl number, the Hartmann number due to radial and axial magnetic fields, the Marangoni number and the radii ratio which are defined as below:

$$A = \frac{L}{D}; \quad \mathrm{Ra} = \frac{g\beta(\theta_h - \theta_c)D^3}{\nu\kappa}; \quad \Pr = \frac{\nu}{\kappa};$$

$$\mathrm{Har} = B_{0r}D\sqrt{\sigma_e/\rho\nu}; \quad \mathrm{Hax} = B_{0x}D\sqrt{\sigma_e/\rho\nu};$$

$$\mathrm{Ma} = -\frac{\partial\sigma}{\partial\theta}\frac{(\theta_h - \theta_c)D}{\mu\kappa}; \quad \lambda = \frac{r_o}{r_i}.$$

The overall heat transfer rate across the cavity is given by the average Nusselt number, which is of central importance to many technological applications. The average Nusselt number at the hot wall is defined as

$$\overline{\mathrm{Nu}} = \int_0^1 \mathrm{Nu}\, dX, \quad \text{where } \mathrm{Nu} = -\left.\frac{\partial T}{\partial R}\right|_{R=0}$$

is the local Nusselt number (6)

3. Numerical details and model verification

A finite difference technique based on the two-step Alternating Direction Implicit (ADI) method has been employed to solve the vorticity transport and the energy equations. In order to improve the stability of the numerical scheme and to speed up the convergence, the non-linear convective terms in the ADI method are approximated by second upwind differences. The diffusion terms are approximated using the central differences. On the other hand, the elliptic stream function equation is solved by the Successive Line Over Relaxation (SLOR) method. The discretized algebraic equations are arranged in tri-diagonal matrix form, which can be solved using the Thomas algorithm. Due to addition of magnetic field, the vorticity equation has two additional terms. In order to retain the second order accuracy, these terms are also approximated by the central differences. Finally, the velocity components are evaluated using the central difference approximation to Eq. (4). A uniform grid is used in the calculation domain and all numerical results are checked for the grid independency. The mesh independency test is carried out for both cases, with and without surface tension effects. The variation of average Nusselt number is monitored for a grid system of $41 \times 41, 61 \times 61, 81 \times 81$ and 101×101. To save the computational time and also due to the negligible difference between the results obtained from 81×81 and 101×101 grid systems, a 81×81 grid system for $A = 1$ is used for further calculations. Similar tests were also conducted for other aspect ratios to chose the optimum grid sizes. The solution is considered to converge when the following convergence criterion is satisfied:

$$\frac{\sum_i\sum_j|\Phi_{i,j}^{new} - \Phi_{i,j}^{old}|}{\sum_i\sum_j|\Phi_{i,j}^{new}|} \leqslant \Gamma$$

Here Φ is any variable Ψ, η, T and Γ is a pre-specified constant, usually set to 10^{-6}.

3.1. Numerical model verification

To verify the numerical method developed for the present simulation, the numerical results are compared with different benchmark solutions available in the literature for the annular and rectangular cavities in the absence of magnetic field and surface tension. Table 1 shows the comparison of average Nusselt number obtained by the present study and that obtained by Kumar and Kalam (1991) for the cylindrical annular enclosure. Further, by putting $D = 0$ in the governing equations (rectangular cavity) of the present study, the average Nusselt number is measured along the hot wall of the cavity. The quantitative results are compared with the corresponding solutions of de Vahl Davis (1983), Le Quere and De Roquefort (1985) and Ho and Lin (1997) for the rectangular cavity and are given in Table 2. From Tables 1 and 2, it can be seen that our numerical results agree well with the earlier investigations over the entire range of Rayleigh numbers, with maximum error less than 1.05%.

4. Results and discussion

The effect of axial and radial magnetic fields on the combined buoyancy and surface tension driven convection of an electrically conducting fluid is numerically investigated in an annular enclosure. The numerical simulations are carried out for a wide range of physical and geometrical parameters like Rayleigh number ($10^3 \leqslant \mathrm{Ra} \leqslant 10^6$), Marangoni number ($10^2 \leqslant \mathrm{Ma} \leqslant 10^5$), Hartmann number due to radial and axial magnetic fields ($0 \leqslant \mathrm{Har}, \mathrm{Hax} \leqslant 100$) and radii ratio ($1 \leqslant \lambda \leqslant 10$) in an annular enclosure with aspect ratio $A = 0.5$, 1 and 2. The Prandtl number is fixed at 0.054, which corresponds to liquid metals and semi-conductor melts. The flow and temperature fields inside the annular enclosure are presented in terms of the streamlines and isotherms. The rate of heat transfer at the hot wall is estimated from the average Nusselt number. The main aim of the present study is to investigate the interplay between the magnetic, buoyancy and thermocapillary forces at different values of the physical parameters of the problem.

Table 1
Comparison of present results with annular cavity for $A = 1$ and $\lambda = 2$.

	Kumar and Kalam (1991)	Present study
$\mathrm{Ra} = 10^4$	3.3047	3.3064
$\mathrm{Ra} = 10^5$	6.2681	6.2695
$\mathrm{Ra} = 10^6$	11.8889	11.8932

Table 2
Comparison of present results with rectangular cavity ($\lambda = 1$) for $A = 1$.

Ra		de Vahl Davis (1983)	Le Quere and De Roquefort (1985)	Ho and Lin (1997)	Present study
10^3	Nu	1.116	1.118	1.118	1.117
	$\lvert\Psi\rvert_{max}$	1.174	1.175	–	1.175
	V_{max}	3.696	3.697	3.697	3.698
10^4	Nu	2.243	2.245	2.248	2.247
	$\lvert\Psi\rvert_{max}$	5.081	5.074	–	5.077
	V_{max}	19.64	19.63	19.63	19.641
10^5	Nu	4.517	4.522	4.528	4.521
	$\lvert\Psi\rvert_{max}$	9.121	9.619	–	9.617
	V_{max}	68.68	68.64	68.63	68.627
10^6	Nu	8.797	8.825	8.824	8.806
	$\lvert\Psi\rvert_{max}$	16.41	16.81	–	16.421
	V_{max}	221.13	220.6	219.86	221.63

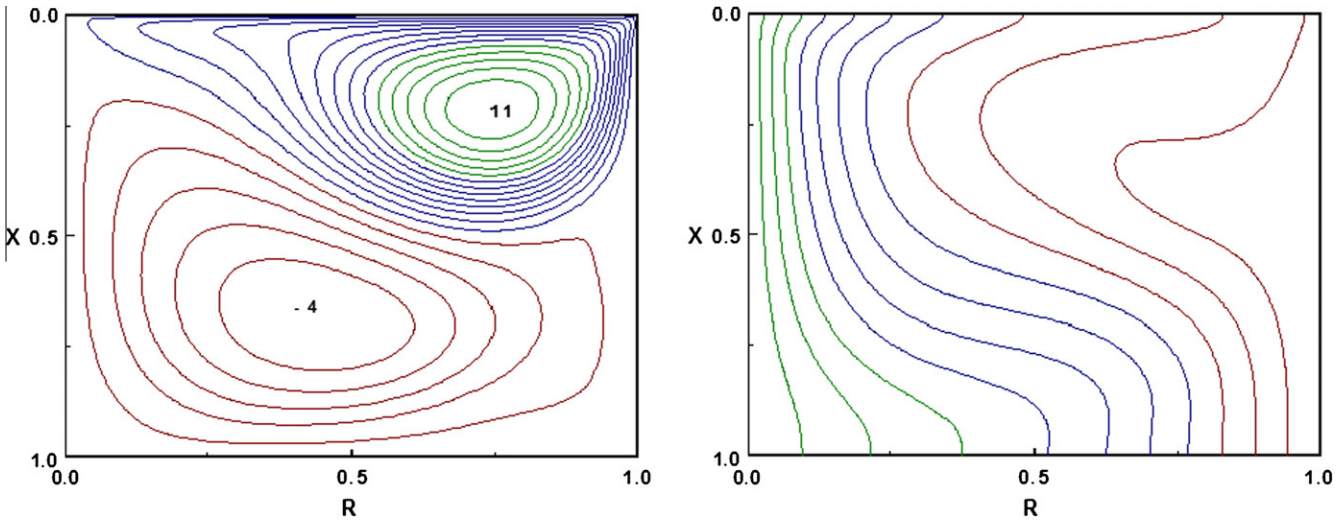

Fig. 2. Streamlines and isotherms for Har = Hax = 0, Ra = 10^4, Ma = 10^5, A = 1 and λ = 2.

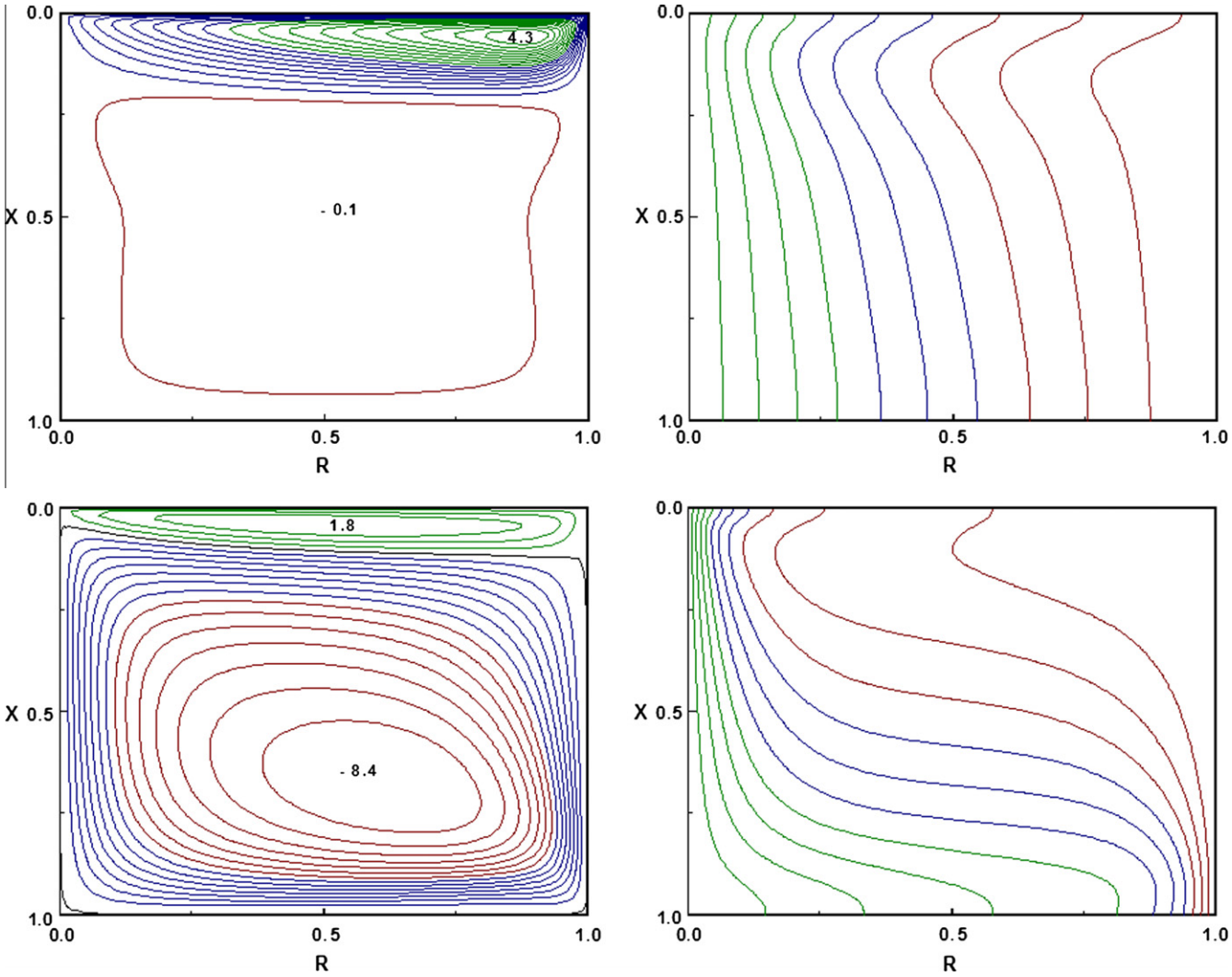

Fig. 3. Effect of radial magnetic field on the streamlines and isotherms for Har = 100, Hax = 0, Ma = 10^5, A = 1 and λ = 2, (upper) Ra = 10^4 and (lower) Ra = 10^6.

4.1. Effect of magnetic field in a square annulus

The hydrodynamic flow and thermal fields inside the annular enclosure are exemplified by the streamlines and isotherms in Fig. 2 in the absence of radial and axial magnetic fields. The basic mechanism related with the flow generated by the buoyancy and thermocapillary forces are strongly different from each other. The thermocapillary effect is a surface tension driven phenomenon,

and hence it primarily affects the flow near the free surface of the annulus. On the other hand, the buoyancy driven convection is caused by the temperature gradients present in the fluid, and as a result, its effects are distributed in the bulk of the flow field. Fig. 2 illustrates the interaction of these two forces at different values of the chosen parameters. Since the value of Rayleigh number is lower, compared to the Marangoni number, the flow field in the annulus is mainly dominated by the surface tension mechanism as indicated by the strong anti-clockwise rotating flow near the free surface. Also, the flow is strongly divided into two regions; an upper vortex, where the motion is induced by the surface tension, and the lower vortex is driven by the buoyancy force (Fig. 2). When the buoyancy and thermocapillary forces are of equal strength, the surface tension driven cell reduces in size and the buoyancy driven cell grows stronger, and as the Rayleigh number increases, a strong flow driven by the buoyancy force exists in the annular enclosure. This is due to the increasing role played by the buoyancy force that gradually overcomes the effect of thermocapillary force in the cavity.

As regards to the effect of magnetic field on the flow and thermal distributions in the square annulus, two different combinations of Rayleigh and Marangoni numbers are considered in Figs. 3 and 4. The values of these two parameters are chosen in such a way that the influence of buoyancy force is meager (Ra < Ma) and dominant (Ra > Ma) to the thermocapillary force. The influence of radial magnetic field strength (Har = 100) on the streamlines and isotherms is shown in Fig. 3. For Ra = 10^4, the dominant flow in the annulus is due to the thermocapillary force. The flow is mainly developed near the free surface and a large vortex located in the upper region of the cavity is dominating the flow structure as shown in Fig. 3(upper). The isotherms near the free surface confirm a similar behavior, as they move towards the hot wall, due to strong thermocapillary effect. In the middle of the annulus, a weak flow driven by the buoyancy force exists. From Fig. 3(upper), it can be seen that the buoyancy driven convection is almost suppressed by the strong radial magnetic field, which is further supported by the nearly-parallel isotherms in the middle of the annulus. On comparing Fig. 2, the magnitude of maximum stream function of the thermocapillary and buoyancy driven cell is reduced due to the damping effect produced by the radial magnetic field.

It is worth to mention that the Marangoni number can be assigned with a positive or negative sign. The positive value of the Marangoni number augments the buoyancy driven convection, whereas a negative Marangoni number opposes the natural convection. In the present study, the Marangoni number is associated with a negative sign, and thereby the surface tension forces counteract with the buoyancy forces. That is, the buoyancy force has to overcome the two opposing forces, namely the thermocapillary force and the Lorentz force due to the applied magnetic field. Hence, the buoyancy driven flow is strongly suppressed by the

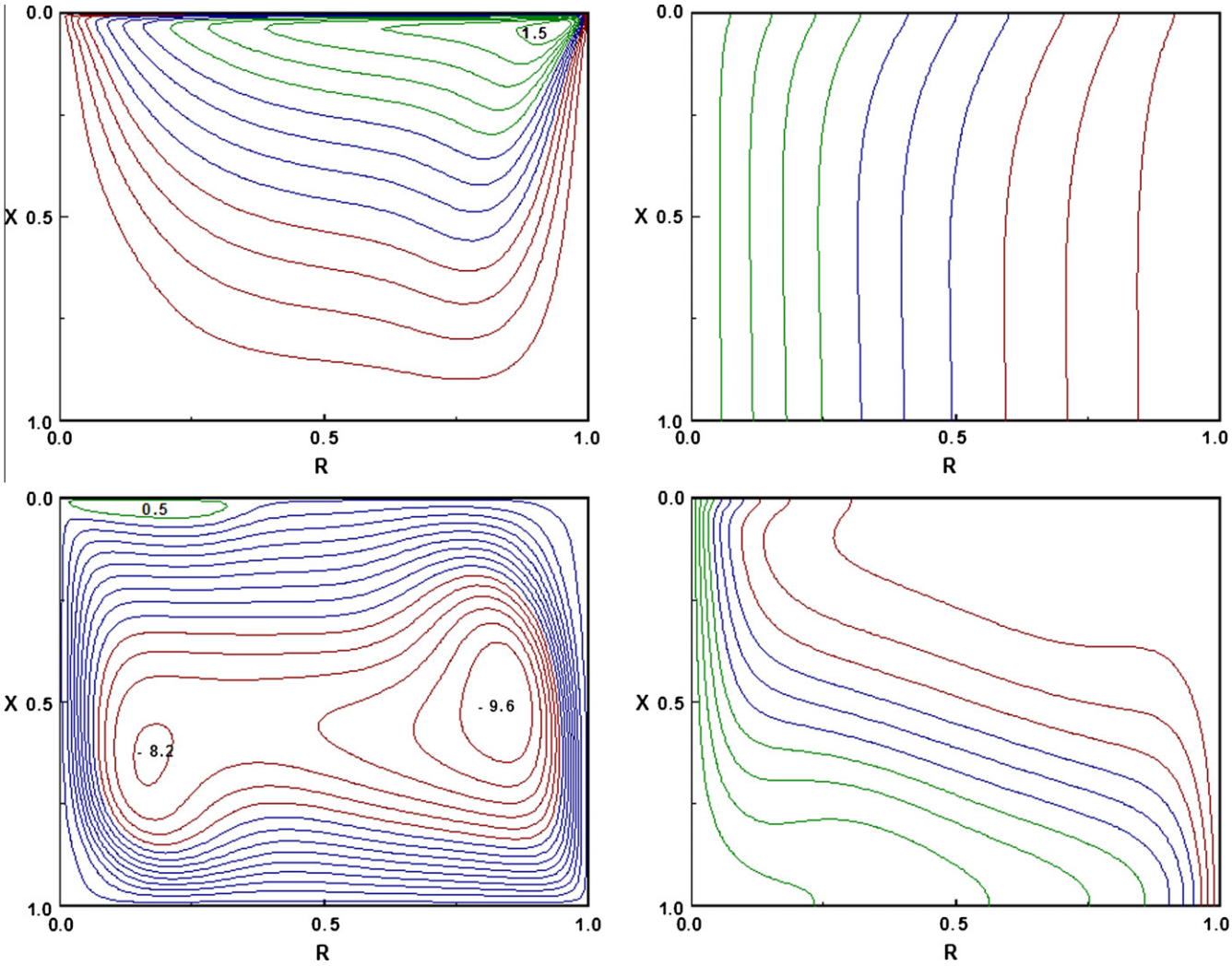

Fig. 4. Effect of axial magnetic field on the streamlines and isotherms for Har = 0, Hax = 100, Ma = 10^5, $A = 1$ and $\lambda = 2$, (upper) Ra = 10^4 and (lower) Ra = 10^6.

magnetic field at a small value of Rayleigh number. When the buoyancy and thermocapillary forces are equal in magnitude, the buoyancy force overcomes the counteracting thermocapillary and magnetic forces, and the buoyancy driven cell exists near the middle of the annulus with the same strength as that of the surface tension driven cell. However, as the Rayleigh number increases, the buoyancy force dominates over the thermocapillary forces, and a strong buoyancy driven flow prevails in the annulus. The isotherms reveal the temperature stratification in the annulus, the magnetic field mainly suppresses the surface tension driven flow (Fig. 3 lower).

The influence of an axial magnetic field (Hax = 100) on the streamline and isotherm pattern is illustrated in Fig. 4. For the case of Ma > Ra, due to the enhanced thermocapillary effect, the strength of surface tension driven convection outweighs the buoyancy driven convection in the annulus (Fig. 4 upper). The stronger axial magnetic field completely suppresses the buoyancy driven flow, and the surface tension driven convection is also suppressed up to some extent. The less distorted isotherms signify the low convective heat transfer. However, as the Rayleigh number is increased to 10^6, a symmetric buoyancy driven flow exists with two vortices at the centre of the annular cavity. For the same set of parameters, compared to the radial magnetic field, the suppression of flow strength and temperature stratification is found to be higher for the case of an axial magnetic field. In particular, the surface tension driven flow is suppressed noticeably, as compared to the radial magnetic field case (Figs. 3 and 4). This is reasonable to expect, since the flow driven by the thermocapillary forces are mainly confined to a smaller region near the top free surface, and moves along the free surface. Thus, the direction of surface tension flow is perpendicular to the axial magnetic field, and hence the flow is suppressed more effectively by the axial magnetic field than the radial magnetic field. As the Rayleigh number is increased to 10^6, the major portion of the annulus is occupied by the buoyancy driven flow, and the surface tension flow is confined to a tiny region near the top free surface (Fig. 4 lower). The nearly-parallel

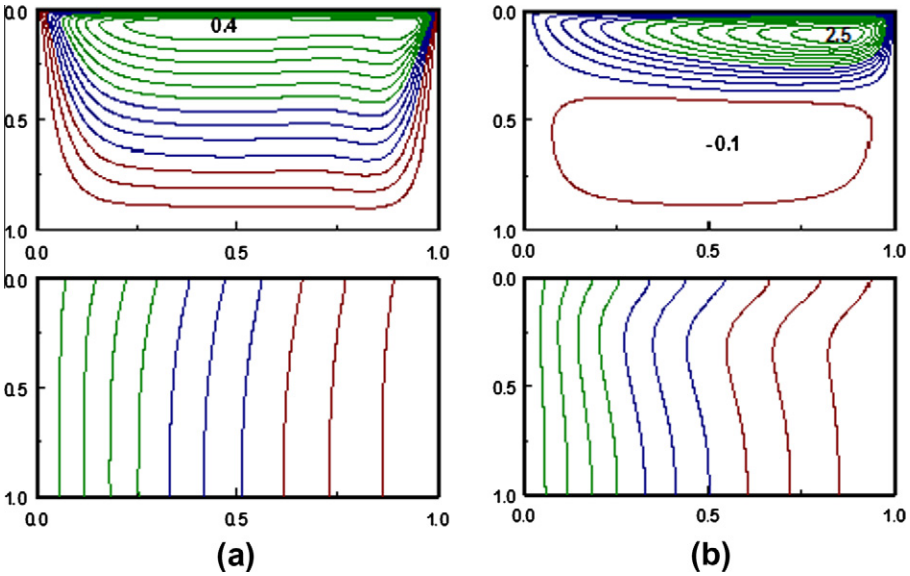

Fig. 5. Effect of (a) axial and (b) radial magnetic fields on the streamlines and isotherms for $A = 0.5$, $\lambda = 2$, $Ra = 10^4$ and $Ma = 10^5$. In figure (a) Har = 0 and Hax = 100 and in (b) Har = 100 and Hax = 0.

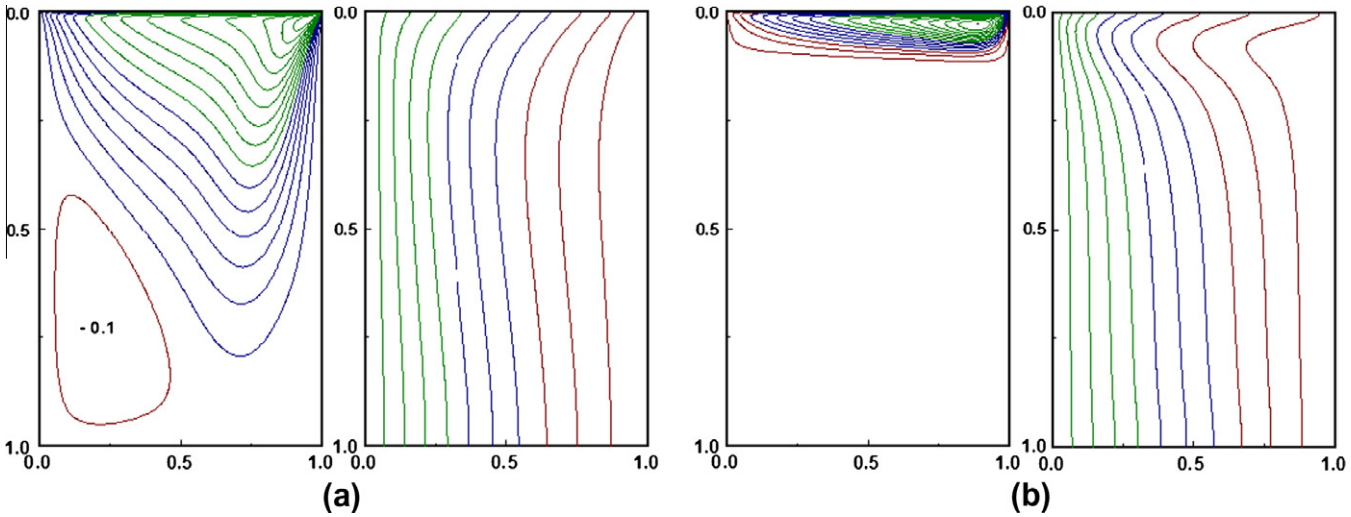

Fig. 6. Effect of (a) axial and (b) radial magnetic fields on the streamlines and isotherms for $A = 2$, $\lambda = 2$, $Ra = 10^4$ and $Ma = 10^5$. In figure (a) $\Psi_{max,s} = 2.6$, Har = 0 and Hax = 100 and in (b) $\Psi_{max,s} = 7.0$, Har = 100 and Hax = 0.

isotherms, for Ra < Ma, show a considerable variation towards the hot wall, due to the presence of strong buoyancy driven convection.

4.2. Effect of magnetic field in a shallow and tall annulus

The variations in the flow pattern and temperature distribution with respect to aspect ratio will be of much interest, when aspect ratio of the annulus changes from unity, and are given in Figs. 5 and 6 for Ra = 10^4 and Ma = 10^5 as a representative case. In the shallow annulus, since the Rayleigh number is less than the Marangoni number, the thermocapillary effects are stronger relative to the effects due to buoyancy force, and hence the annulus is mainly occupied with surface tension driven cell (Fig. 5). The streamline and isotherm pattern indicates that the buoyancy driven convection is completely suppressed by the axial magnetic field, when the Marangoni number is higher than the Rayleigh number. But, as the Rayleigh and Marangoni numbers are equal, the buoyancy driven convection begins to exist in the cavity and accelerates the flow in clockwise direction. Furthermore, when Ra > Ma, the buoyancy driven convection outweighs the thermocapillary convection, and hence the entire annular cavity is filled with the buoyancy driven flow. For the same set of parameters, if the flow and thermal fields are compared between the radial and axial magnetic fields, one can clearly observe that the flow and heat transfer in the annular cavity is more effectively suppressed by the axial magnetic field rather than the radial magnetic field (Fig. 5). Another important observation that can be made from Fig. 5 is that the surface tension flow is effectively suppressed by the axial magnetic field compared to the radial magnetic field. This

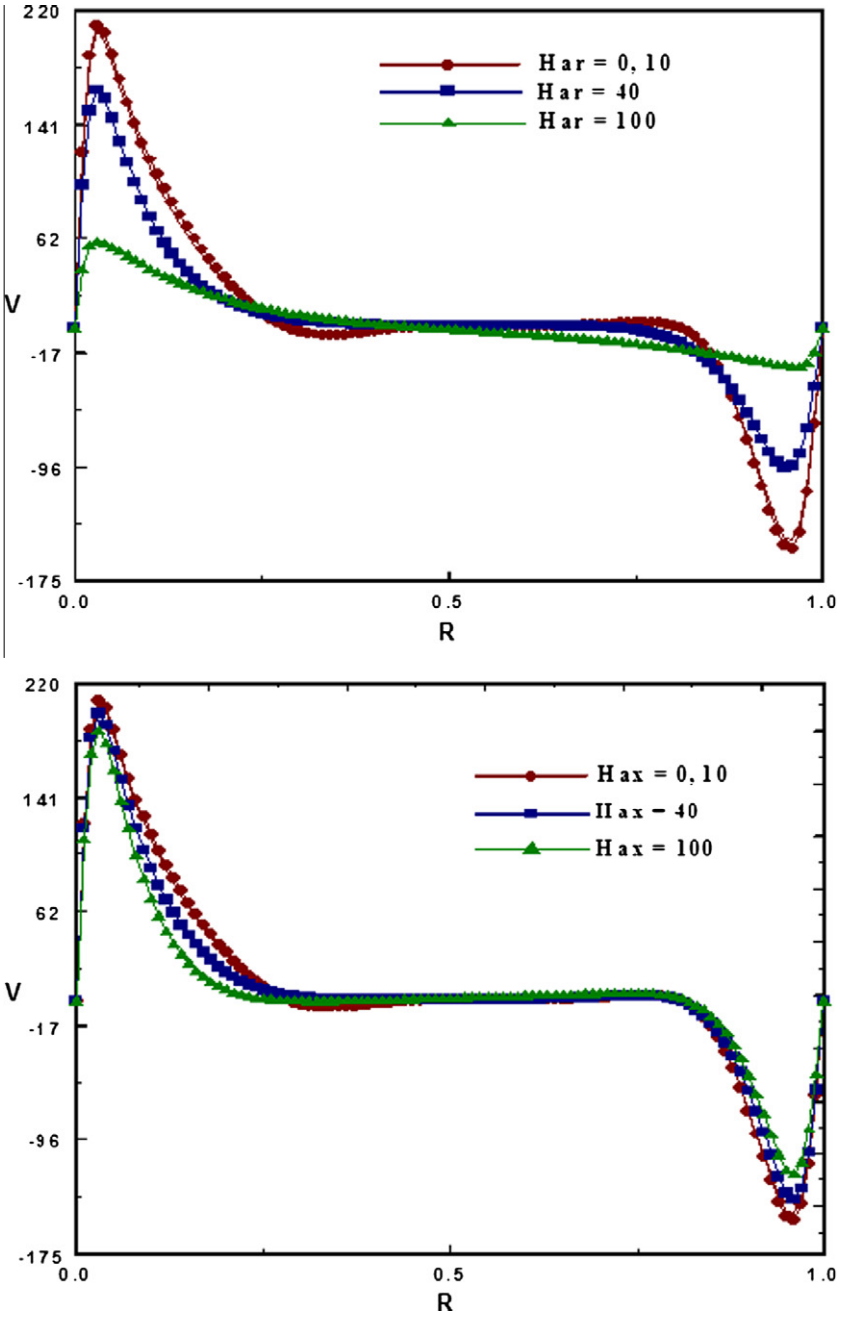

Fig. 7. Effect of radial and axial magnetic fields on the axial velocity at the mid-height of the annular cavity for Ra = 10^6, Ma = 10^4, $\lambda = 2$ and $A = 2$.

is due to the fact that the external magnetic field suppresses the flow more effectively when its direction is normal to the main flow. In a shallow annulus, the main flow will be along the horizontal direction, and hence the convective flow can be efficiently suppressed by an axial magnetic field.

The effect of axial and radial magnetic fields on the flow pattern and temperature distribution in a tall annulus ($A = 2$) is shown in Fig. 6. Since the buoyancy force is smaller, the stabilizing effect of magnetic field dominates over the destabilizing effect of buoyancy, while the opposite holds if the magnitude of the temperature gradient is sufficiently large. When the surface tension force is higher than the buoyancy force, the existence of buoyancy driven cell depends on the direction of magnetic field. For the axial magnetic field, a weak buoyancy driven cell exists near the bottom, whereas its existence is suppressed for the case of radial magnetic field. A careful observation of Fig. 6 reveals that the magnitude of $|\Psi_{max,s}|$, which determines the strength of surface tension flow, is relatively higher for the case of radial magnetic field compared to the axial magnetic field. Also, when the radial magnetic field is applied, the surface tension driven flow is confined to a smaller region along the free surface. Though the area occupied by the surface tension flow is smaller, it exhibits a greater flow velocity along the free surface (Fig. 6b). This indicates that the axial (radial) magnetic field suppresses the surface tension (buoyancy) flow more effectively than the radial (axial) magnetic field. Thus, it can be concluded that the magnetic field suppresses the flow more effectively when it is applied perpendicular to the flow direction. Fig. 7 exemplifies the effect of radial and axial magnetic fields on the vertical velocity profiles at the mid-height of the annulus ($X = 0.5$) for different values of Har, Hax and $A = 2$. The effect of magnetic field

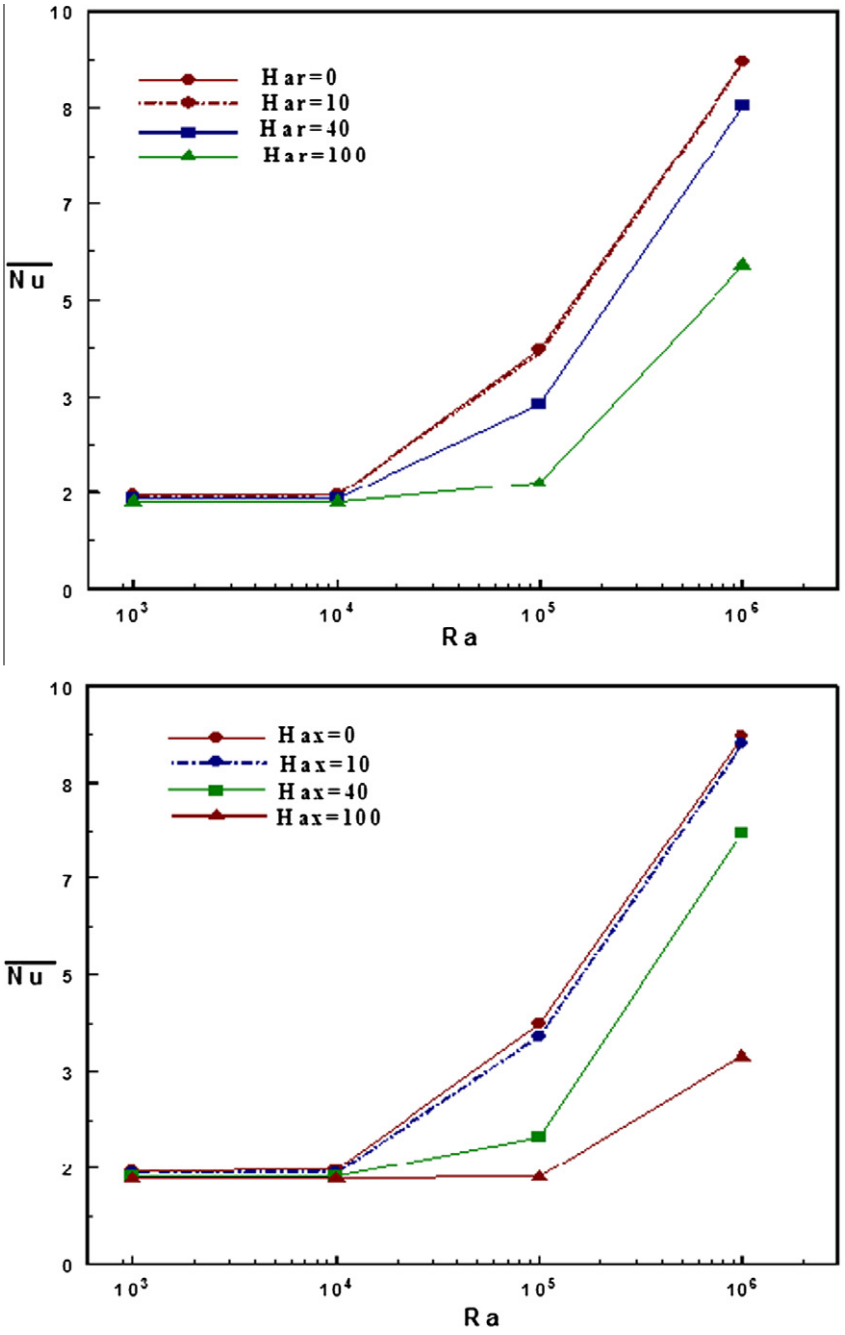

Fig. 8. Effect of radial and axial magnetic fields on the average Nusselt number for $Ra = 10^6$, $Ma = 10^4$, $\lambda = 2$ and $A = 0.5$.

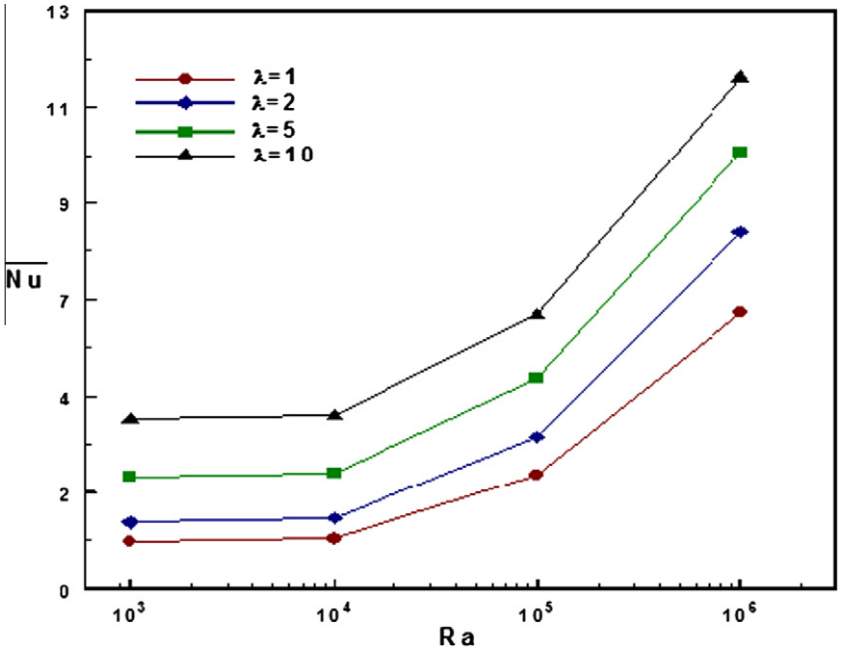

Fig. 9. Effect of radii ratio λ on the average Nusselt number for $A = 1$, Har = 40, Hax = 0 and Ma = 10^3.

on the flow velocity is more evident from these profiles as they change appreciably when Har and Hax increases. In particular, since the annulus is tall, the axial velocity is more effectively suppressed by the radial magnetic field than the axial magnetic field. The figure reveals that the axial velocity decreases with the Hartman number in radial direction, which indicates that the convective intensity is reduced and the heat transfer between the two side walls is dominated by heat conduction gradually.

4.3. Effect of magnetic field on heat transfer

Fig. 8 illustrates the variation of average Nusselt number for different values of Har, Hax in a shallow annulus ($A = 0.5$). From the figure, it can be ascertained that the suppression of heat transfer is more in the case of an axial magnetic field compared to the radial magnetic field. This reveals the fact that the heat transfer in shallow enclosures can be effectively suppressed by applying an axial magnetic field rather than a radial magnetic field. The important geometrical parameter in the annular enclosure is its curvature effect and is given by the non-dimensional parameter namely, the radii ratio. For the sake of brevity, the effect of radii ratio on the streamline and isotherm plots are omitted. In order to have a better understanding of the radii ratio on the heat transfer from the hot wall, the rate of heat transfer along the hot wall is measured in terms of the average Nusselt number $\overline{Nu}$ and is depicted in Fig. 9 at different values of Rayleigh number and radii ratio. The effect of radii ratio on the average heat transfer rate is apparent from Fig. 9 at all Rayleigh numbers. Introduction of curvature effect increases the average Nusselt number on the inner wall. This is mainly due to the modification of temperature and velocity fields in the annulus. The boundary layer temperature profiles are strongly affected and a lower sink temperature for the inner boundary layer results as the radius ratio is increased. However, it is observed that the heat transfer rate decreases at all radii ratios, when the magnetic field is applied to the flow.

5. Conclusions

Numerical computations has been carried out to assess the effect of a radial or axial magnetic field on the combined buoyancy and surface tension driven convection in a cylindrical annular cavity by solving the Navier–Stokes equations for a wide range of physical parameters. From the results presented, the following main conclusions are drawn:

- For smaller and moderate Rayleigh numbers, the buoyancy driven convective flow has been controlled effectively by the magnetic field. On the contrary, for high Rayleigh number, the magnetic field is effective in suppressing the thermocapillary driven convective flow in the annulus.
- The magnetic field is more effective in suppressing the heat transfer when it is perpendicularly applied to the direction of the primary flow. That is, in shallow cavities, the axial magnetic field is found to be better in controlling the flow and heat transfer.
- In tall cavities, the axial magnetic field suppresses the surface tension flow more effectively than the radial magnetic field. On the contrary, the radial magnetic field is found to be better in suppressing the buoyancy driven flow compared to axial magnetic field.
- The quantitative results, presented in terms of the average Nusselt number, indicate that the heat transfer rate increases with radii ratio and decreases with the Hartmann number.
- From the results, we also found that the surface tension effect is predominant in the shallow cavities compared to the square and tall annulus. Further, The surface tension forces induces a bicellular flow in shallow and square enclosures.

Acknowledgement

M. Venkatachalappa was supported by UGC under CAS Programmes, and M. Sankar and Y. Do were supported by WCU (World Class University) program through the Korea Science and Engineering Foundation funded by the Ministry of Education, Science and Technology (Grant No. R32-2009-000-20021-0). The author M. Sankar would like to acknowledge the support and encouragement of Chairman and Principal of EPCET, Bangalore, India.

References

Alboussière, T., Garandet, J.P., Moreau, R., 1996. Asymptotic analysis and symmetry in MHD convection. Phys. Fluids 8, 2215–2226.

Bauer, H.F., Eidel, W., 2007. Thermocapillary convection in an annular cylindrical container. Heat Mass Transfer 43, 217–232.

BenHadid, H., Henry, D., 1997. Numerical study of convection in the horizontal Bridgman configuration under that action of a constant magnetic field. Part2. Three-dimensional flow. J. Fluid Mech. 333, 57–83.

Bergman, T.L., Ramadhyani, S., 1986. Combined buoyancy and thermocapillary driven convection in open square cavities. Numer. Heat Transfer, Part A 9, 441–451.

Bergman, T.L., Keller, J.R., 1988. Combined buoyancy, surface tension flow in liquid metals. Numer. Heat Transfer, Part A 13, 49–63.

Carpenter, B.M., Homsy, G.M., 1989. Combined buoyant thermocapillary flow in a cavity. J. Fluid Mech. 207, 121–132.

de Vahl Davis, G., 1983. Natural convection of air in a square cavity: a bench mark numerical solution. Int. J. Numer. Methods Fluids 3, 249–264.

Garandet, J.P., Alboussière, T., Moreau, R., 1992. Buoyancy-driven convection in a rectangular enclosure with a transverse magnetic field. Int. J. Heat Mass Transfer 35, 741–748.

Gelfgat, A.Y., Bar-Yoseph, P.Z., 2001. Effect of an external magnetic field on oscillatory instability of convective flows in rectangular cavity. Phys. Fluids 13, 2269–2278.

Ha, E.J., Kim, W.S., 2005. A study of low-power density laser welding process with evolution of free surface. Int. J. Heat Fluid Flow 26, 613–621.

Ho, C.J., Lin, F.H., 1997. Simulation of natural convection in a vertical enclosure by using a new incompressible flow formulation: pseudovorticity–velocity formulation. Numer. Heat Transfer, Part A 31, 881–896.

Hossain, A., Hafizb, M.Z., Rees, D.A.S., 2005. Buoyancy and thermocapillary driven convection flow of an electrically conducting fluid in an enclosure with heat generation. Int. J. Therm. Sci. 44, 676–684.

Juel, A., Mullin, T., Ben Hadid, H., Henry, D., 1999. Magnetohydrodynamic convection in molten gellium. J. Fluid Mech. 378, 97–118.

Kakarantzas, S.C., Sarris, I.E., Grecos, A.P., Vlachos, N.S., 2009. Magnetohydrodynamic natural convection in a sinusoidal upper heated cylindrical cavity. Int. J. Heat Mass Transfer 52, 250–259.

Kamotani, Y., Lee, J.H., Ostrach, S., 1992. An experimental study of oscillatory thermocapillary convection in cylindrical containers. Phys. Fluids A4 (5), 955–962.

Kim, Y.-D., Kim, W.-S., 2008. A numerical analysis of heat and fluid flow with a deformable curved free surface in a laser melting process. Int. J. Heat Fluid Flow 29 (5), 1481–1493.

Kobayashi, S., 1986. Effects of an external magnetic field on source distribution in Czochralski grown crystals – a theoretical analysis. J. Crystal. Growth 75, 301–308.

Kumar, R., Kalam, M.A., 1991. Laminar thermal convection between vertical co-axial isothermal cylinders. Int. J. Heat Mass Transfer 34 (2), 513–524.

Langlois, W.E., 1985. Buoyancy-driven flows in crystal growth melts. Ann. Rev. Fluid Mech. 17, 191–215.

Le Quere, P., De Roquefort, T.A., 1985. Computation of natural convection in two dimensional cavity with chebyshev polynomials. J. Comp. Phys. 57, 210–228.

Lee, S.H., Hyun, J.M., 2005. Transient buoyant convection of air in an enclosure under strong magnetic effect. Int. J. Heat Mass Transfer 48, 3097–3106.

Moessner, R., Mueller, U., 1999. A numerical investigation of three dimensional magneto-convection in rectangular cavities. Int. J. Heat Mass Transfer 42, 1111–1121.

Moreau, R., 1998. Magnetohydrodynamics. Kluwer Academic, London.

Ozoe, H., Okada, H., 1989. The effect of the direction of the external magnetic field on the three-dimensional natural convection in a cubic enclosure. Int. J. Heat Mass Transfer 32, 1939–1954.

Roache, P.J., 1972. Computational Fluid Dynamics. Hermosa, Albuquerque, NM.

Rudraiah, N., Venkatachalappa, M., Subbaraya, C.K., 1995. Combined surface tension and buoyancy-driven convection in a rectangular open cavity in the presence of a magnetic field. Int. J. Non-Linear Mech. 30 (5), 759–770.

Sankar, M., Venkatachalappa, M., Shivakumara, I.S., 2006. Effect of magnetic field on natural convection in a vertical cylindrical annulus. Int. J. Eng. Sci. 44, 1556–1570.

Sarris, I.E., Kakarantzas, S.C., Grecos, A.P., Vlachos, N.S., 2005. MHD natural convection in a laterally and volumetrically heated square cavity. Int. J. Heat Mass Transfer 48, 3443–3453.

Sarris, I.E., Zikos, G.K., Grecos, A.P., Vlachos, N.S., 2006. On the limits and validity of the low magnetic Reynolds number approximation in MHD natural convection heat transfer. Numer. Heat Transfer, Part B 50, 157–180.

Schwabe, D., Zebib, A., Sim, B.-C., 2003. Oscillatory thermocapillary convection in open cylindrical annuli. Part 1. Experiments under microgravity. J. Fluid Mech. 491, 239–258.

Schwabe, D., 1988. Surface-tension-driven flow in crystal growth melts. Crystals 11, 75–112.

Sim, B.-C., Zebib, A., Schwabe, D., 2003. Oscillatory thermocapillary convection in open cylindrical annuli. Part 2. Simulations. J. Fluid Mech. 491, 259–274.

Srinivasan, J., Basu, B., 1986. A numerical study of thermocapillary flow in a rectangular cavity during laser melting. Int. J. Heat Mass Transfer 29, 563–572.

Strani, M., Piva, R., Graziani, G., 1983. Thermocapillary convection in a rectangular cavity: asymptotic theory and numerical simulation. J. Fluid Mech. 130, 347–376.

Venkatachalappa, M., Subbaraya, C.K., 1993. Natural convection in a rectangular enclosure in the presence of a magnetic field with uniform heat flux from the side wall. Acta Mech. 96, 13–26.

Vrentas, J.S., Narayana, R., Agrawal, S.S., 1981. Free surface convection in a bounded cylindrical geometry. Int. J. Heat Mass Transfer 24, 1513–1529.